The Molecular Weight Dependence of Nuclear Spin Correlations in Entangled Polymeric Liquids

P. T. Callaghan[†] and E. T. Samulski*[,‡]

Department of Physics, Massey University, Palmerston North, New Zealand, and Department of Chemistry, University of North Carolina at Chapel Hill, Chapel Hill, North Carolina 27599-3290

Received October 14, 1997; Revised Manuscript Received February 10, 1998

ABSTRACT: We present experimental proton NMR data for poly(dimethylsiloxane) (PDMS) and poly(ethylene oxide) (PEO) in the form of a β-echo (sine correlation) function which is particularly sensitive to modulations of nuclear dipolar interactions caused by slow molecular reorientations in entangled melts. Theoretical expressions for the β-echo can be computed with a closed-form expression that depends on the correlation function describing macromolecular motion. We use a simple correlation function for reptation that depends on only two parameters, $\bar{M}_2$, the pre-averaged dipolar interaction strength and τ_d, the tube disengagement time. From fits of the molecular weight dependence of the proton NMR measurements of β in PDMS melts at 300 K, we conclude that the classical reptation model ($\tau_d \sim M^z$ where $z = 3$) applied to the decay of residual intramolecular dipolar interactions is applicable in high molar mass melts ($M \geq 500\,000$) but intermolecular interactions, described by a lower molar mass scaling process (M^z, $z = 1-2$), dominate the data for smaller (entangled) chains. The temperature dependence of τ_d suggests an Arrhenius behavior with an activation energy of 13 kJ mol^{-1}, the same as that observed for bulk viscosity. PEO appears to exhibit dynamics dominated by processes with a smaller scaling exponent.

Introduction

In what was perhaps the first NMR study of poly(dimethyl siloxane) melts, Powles *et al.*[1] reported in 1961 that the more viscous fluids—the high molar mass polymers—exhibited a transverse decay of nuclear spin magnetization that was nonexponential. This observation was interpreted to mean that the proton NMR signal from the melt had characteristics of a broad line despite the fact that, in terms of absolute frequency spread, it was narrow. Similar observations were noted in other polymer melts and the term "narrow broad" lines was proposed to describe this behavior; it was thought to be characteristic of the proton NMR of fluids composed of long chain compounds.[2] Moreover, Powles et al. posited that this peculiar line shape was the result of "some magnetic interaction between the spins which has a correlation frequency much less than the Larmor frequency." They speculated that the intramolecular direct dipole−dipole interaction between a pair of protons was the relevant interaction. Additionally, they suggested that this dipolar interaction was weak because the (rigid lattice) dipolar interaction was motionally averaged: the orientation-dependent local dipolar field is modulated by molecular dynamics. In sum, the consequences and the origins of nuclear spin correlations in viscous polymer melts was recognized almost 4 decades ago. Herein we quantitatively measure the residual dipolar interactions in polymer melts as a function of chain length and interpret our findings in terms of contemporary models of polymer dynamics in entangled melts.

In the 1970s after de Gennes emphasized the role of entanglement topology in his reptation model of polymer dynamics,[3] Cohen-Addad[4,5] suggested that the weak (residual) proton dipolar interactions could be used to characterize polymer melts and networks. To this end, we recently introduced[6] a specially tailored NMR spin-echo function, β, that is inherently sensitive to the weak dipolar interactions and thereby capable of delineating slow, cooperative multichain processes. This spin-echo function was shown to be directly related to terms in the nuclear spin Hamiltonian which contain information about local order and dynamics. Subsequently Ball, Callaghan, and Samulski (BCS) showed that the time dependence of β could be calculated if one had information concerning the strength of the local residual dipolar interactions in addition to a knowledge of the correlation function which expressed their temporal fluctuations.[7] In particular, BCS proposed a new correlation function, based on the tube model of reptation[1,8] in entangled polymer fluids, that explicitly accounts for the averaging of dipolar interactions. In conjunction with closed-form expressions for β, BCS illustrated how relevant orientational correlation functions which explicitly represent the key physical processes underlying reptation such as tube disengagement can yield analytic solutions to experimental parameters. In this paper we use their findings to quantitatively interpret the MW dependence observed for proton NMR determinations of β in entangled melts, taking as examples poly(dimethyl siloxane) and poly(ethylene oxide).

Theoretical Background

NMR and the Spin Hamiltonian. When a polymeric fluid is placed in a strong magnetic field, the protons at the hydrogen sites interact with their environment through a number of specific interactions which are represented by terms in the so-called "spin Hamiltonian". The principal interaction is that of the nuclear dipole with the external field, the Zeeman interaction. This term contains a number of subtle variants, depending on the local electron cloud surrounding the nucleus (the chemical shift), on the polarizing field quality (the field inhomogeneity), and on the

[†] Massey University.
[‡] University of North Carolina at Chapel Hill.

S0024-9297(97)01502-7 CCC: $15.00
Published on Web 05/15/1998

sample geometry (the diamagnetic susceptibility inhomogeneity). The first of these three is the (generally) desirable basis of identification of chemical primary structure in NMR spectroscopy while the second and third are generally considered undesirable factors. Field inhomogeneity is minimized by careful "shimming" while susceptibility inhomogeneity effects will be absent in cylindrically or spherically shaped samples of uniform consistency but is unavoidable in the presence of sample irregularity, interior voids, or devices for studying the sample rheology.

Another category of Hamiltonian terms experienced by the proton concerns those due to direct or indirect interactions between the spins. These include the through-space dipolar interaction and the electron-mediated spin−spin or scalar (*J*-coupling) interaction. While both of these are characterized by bilinear spin operators, the former is intrinsically strong in magnitude (≥100 kHz for nearby hydrogen nuclei) and has the rotational properties of a rank-two tensor while the second is intrinsically weak (≤100 Hz) and rotationally invariant.[9] It is the dipolar interaction which will concern us in this paper. In particular we note that for small molecules tumbling much more rapidly than the dipolar interaction strength the modulation of this interaction—its erratic change in magnitude and sign—results in an averaging to zero, the basis of the fact that such interactions may be ignored in high-resolution NMR of liquids. However, in the case of polymeric fluids, the rapid motions (local segmental reorientations) may not be able to completely motionally average the dipolar interaction. In such cases slower reorientations (large-scale chain reconfigurations) are required to complete the motional average. Moreover, the slower motions in entangled polymeric fluids may modulate the residual dipolar effects—the pre-averaged (by rapid local motion) dipolar interaction—at a rate which is distinctly observable in an NMR experiment.

There exists therefore the possibility that weak residual dipolar interactions might be used as a probe of slow polymer dynamics. First however, it is essential to be able to "read" these interactions in an unambiguous manner and without the masking effects of remaining terms in the spin Hamiltonian. Indeed, given a desire to focus on these subtle dipolar effects, all the remaining spin interactions can be considered undesirable. In particular we shall wish to remove the residual Zeeman heterogeneity arising from chemical shifts, from external field inhomogeneity, and from internal susceptibility inhomogeneity effects, the latter being a special problem for viscous melts where interior microvoids may be expected.[10] The technique to be used in this work specifically banishes such effects by giving us an NMR signal which arises only from terms in the Hamiltonian which are bilinear in the spin operators. To that end the scalar spin−spin interaction will be regarded as a nuisance. Fortunately it is either entirely absent (the case where all hydrogen sites are chemically equivalent), sufficiently weak that we may ignore it, or at worst a residual "baseline" which may be identified by performing an experiment with low molar mass, rapidly tumbling polymers for which dipolar interactions are entirely negligible. Only experimental examples for which scalar interactions are absent will be presented in this article.

Spin-Echoes and Dipolar Interactions. Following a 90° rf pulse, the nuclear spin magnetization precesses under the influence of the various interaction terms in the spin Hamiltonian, thus leading to a decay of the transverse magnetization as phase coherence is lost. The rate of this *apparent* decay process (T_2^{*-1}) depends on the combined effect of the Hamiltonian terms listed above, and its measurement provides unselective insight regarding the strength of those various interactions. To distinguish the effect of differing terms it is necessary to employ pulse sequences which result in selective evolution sensitivity. In particular the conventional spin-echo sequence refocuses phase shifts which arise from the evolution of the spin system under Zeeman terms in the Hamiltonian, leaving the dipolar interaction precession unperturbed. The echo is formed by applying a 180° rf pulse in phase quadrature, following an initial evolution period τ. After a further period τ following the second pulse, all precession due to Zeeman terms disappears. This ($90^o_x-\tau-180^o_y$) "Hahn echo" sequence,[11] which lies at the heart of our methodology, comprises one of the fundamental tools of pulse NMR techniques.

If the spin-echo signal is measured over a range of τ values, the decay of the echo envelope my be regarded as providing insight regarding the *intrinsic* T_2 relaxation. In the case of polymeric liquids we shall particularly be concerned with the decay caused by fluctuating dipolar interactions. The Hamiltonian describing the dipolar interaction between spins i and j of gyromagnetic ratio γ and separated by an inter-nuclear distance r_{ij} is

$$H_D(t) = -\mu_0\gamma^2\hbar/4\pi r_{ij}^3 \sum_m (-1)^m (24\pi/5)^{1/2} Y_2^m(\theta(t),\phi(t)) T_2^m \quad (1)$$

where the Y_2^m are spherical harmonics of order 2 and component m, while the T_2^m are bilinear products of spin operators.[12] The arguments $(\theta(t),\phi(t))$ describe the orientation of the inter-nuclear vector with the main polarizing field and will fluctuate according to the motion of the molecule bearing the nuclear spins. Note that the overwhelming size of the Zeeman interaction, $-\gamma B_0 I_z$, arising from the polarizing field B_0, means that we should write $H_D(t)$ in a representation which is diagonal in I_z and consider its effect only as a perturbation in first order.

Off-diagonal terms of the dipolar interaction contribute to transitions between eigenstates and, in particular, the T_1 (or longitudinal) relaxation process. While this process can be used to gain insight regarding polymer dynamics, it is most sensitive to high-frequency fluctuations at the Larmor frequency, γB_0, although field cycling experiments in which the magnitude of B_0 is varied can extend the range significantly downward. This aspect of relaxation as it relates to polymers has been covered in detail elsewhere,[13] and we shall not be concerned further with it.

In contrast, the diagonal (secular) elements of the perturbation modulate the precession frequency of the spin coherences and contribute to the loss of phase-coherence associated with transverse relaxation. For such a process the characteristic fluctuation frequency is determined by the dipolar interaction strength itself. We shall find that this magnitude is quite convenient for the study of slow motion in polymer melts. This secular part of the two-spin dipolar interaction may be

written as

$$H_{D0}(t) = \frac{\mu_0\gamma^2\hbar}{4\pi}\frac{1}{r_{12}^3}P_2(\cos\theta(t))[3I_{1z}I_{2z} - \mathbf{I}_1\cdot\mathbf{I}_2] \quad (2)$$

where $P_2(\cos\theta)$ is the second-order Legendre polynomial, $^1/_2(3\cos^2\theta - 1)$. As the segments of a polymer rotate and translate in Brownian motion, the angle $\theta(t)$ fluctuates and, under the influence of $H_{D0}(t)$, the spin magnetization experiences an additional precession $\omega(t)$. Because of the stochastic nature of the processes associated with term $P_2(\cos\theta(t))$, we find it convenient to describe $\omega(t)$ in terms of a second-order correlation function $\langle\omega(t)\omega(0)\rangle$ and its initial value, $\langle\omega(0)^2\rangle$, the second moment of the dipolar line shape, M_2. For a spin pair in the absence of motion, eq 2 leads to[12]

$$M_2 = \frac{9}{20}\left(\frac{\mu_0\gamma^2\hbar}{4\pi}\right)^2\frac{1}{r_{12}^6} \quad (3)$$

Transverse relaxation under the dipolar interaction arises because of the stochastic properties of the nuclear spin system. Using the symbol $\langle ...\rangle$ to represent an ensemble average over this system, one may write down the normalized transverse decay function as

$$G(t) = \langle\exp\{i\int_0^t dt'\,\omega(t')\}\rangle \quad (4)$$

The problem of how to evaluate eq 4 was first handled by Anderson and Weiss[14] who made the assumption that $\omega(t)$ is a Gaussian-distributed process with zero mean and correlation function $C(t) = \langle\omega(t)\omega(0)\rangle$. By this means eq 4 may be evaluated to the order of the second term in a cumulant expansion so that

$$G(t) = \exp(-\,^1/_2\langle\phi(0,t)^2\rangle) \quad (5)$$

where

$$\phi(0,t) = \int_0^t dt'\,\omega(t') \quad (6)$$

and

$$\langle\phi(0,t)^2\rangle = 2\int_0^t dt'\,(t - t')C(t') \quad (7)$$

If the correlation function, $C(t)$, is characterized by a correlation time τ_c, then two extreme limits may be identified. For $M_2\tau_c^2 \gg 1$, the slow motion limit, $G(t)$ decays with Gaussian character as $\exp(-\,^1/_2M_2t^2)$ while for the rapid motion limit ($M_2\tau_c^2 \ll 1$), $G(t)$ is a simple exponential as $\exp(-M_2\tau_c t)$. Between these limits the transverse magnetization decay is monotonic in character, and so the evaluation of the correlation function from its behavior is not at all straightforward.[15] In this paper we shall be concerned with a quite different means of evaluating fluctuations in dipolar interactions via the transverse magnetization, in particular using a specialized echo signal whose character changes markedly over the differing motional regimes.

The β Function. In the early 1970s, Cohen-Addad[7] suggested that weak, rank-2 tensorial interactions present in entangled polymers might be observed in a convenient manner by means of a combination of spin−echo pulse trains, an idea later demonstrated by Collignon *et al.*[16] in the case of proton dipolar and deuterium quadrupole interactions for polyethylene melts. The signal acquired using this combination will be a null in the absence of dipolar interactions and is very sensitive to their fluctuations. However the particular pulse sequence, $\Gamma(t,\tau)$, chosen by these workers suffers from additional Zeeman dephasing effects. We have recently demonstrated[6] a variant of the Cohen-Addad pulse sequence, $\beta(t,\tau)$, which is highly effective.

The experiment relies on a superposition of signals, $[S_1-S_2-S_3]$, where S_1, S_2, and S_3 are the respective signals arising from $(90°_x-\tau-90°_y)$, $(90°_x-\tau-90°_x)$ and $(90°_x-\tau-180°_y)$ spin-echo pulse trains. This superposition signal is obtained using a single pulse sequence under appropriate phase-cycling conditions.[6] The resulting echo function, which we term $\beta(t,\tau)$, is independent of dephasing effects arising from magnetic inhomogeneity or chemical shifts, effects which would normally mask the dipolar interactions in conventional NMR spectroscopy and which prove extremely troublesome in other dipolar echo experiments. For this experiment the relevant ensemble average corresponding to the β-echo signal at $t = 2\tau$ is

$$\beta(2\tau,\tau) = \langle\sin\phi(0,\tau)\sin\phi(\tau,2\tau)\rangle \quad (8)$$

For a Gaussian-distributed process, it may be shown[7] that

$$\langle\sin\phi(0,\tau)\sin\phi(\tau,2\tau)\rangle = \exp(-\langle\phi(0,\tau)^2\rangle)\sinh(\langle\phi(0,\tau)\phi(\tau,2\tau)\rangle) \quad (9)$$

where

$$\langle\phi(0,\tau)\phi(\tau,2\tau)\rangle = \int_0^\tau dt'\,t'C(t') + \int_\tau^{2\tau} dt'\,(2\tau - t')C(t') \quad (10)$$

The time dependence of the $\beta(2\tau,\tau)$ function is particularly interesting. In the short time limit it rises from zero as $M_2\tau^2$, deviating exponentially as $M_2\tau^2\exp(-\tau/\tau_c)$, reaching a maximum whose height depends on the precise form of the correlation function and then decaying back to zero in a manner also characteristic of $C(t)$. We have demonstrated the use of the initial behavior of the β-echo signal in evaluating weak dipolar interactions in natural rubber under various degrees of extension.[6] In these experiments, Zeeman terms in the Hamiltonian arising from chemical shift effects and susceptibility inhomogeneity are particularly troublesome in conventional FID or solid echo measurements but their effects were absent in the β-echo signal.

We now turn our attention to the use of the β experiment in evaluating dipolar fluctuations in polymer melts. While we shall be concerned here with polymers in which there exists only one chemically distinct hydrogen site in the monomer, and hence no proton chemical shift or scalar coupling interaction, we note that microscopic void spaces which are present in polymer melts cause Zeeman broadening[10] whose removal will prove extremely helpful. Furthermore we look ahead to more sophisticated experiments in which we hope to study the dynamics of the polymer melts under shear−rheoNMR. In these measurements the exterior environment of the polymer sample consists of a mechanical rheometer which may be diamagnetically heterogeneous and asymmetric, thus leading to significant susceptibility broadening. The present study represents a first step in the application of a method

which should prove particularly useful in this more ambitious class of experiment.

To apply the method it is important to be able to relate the shape of the β-echo envelope to the key parameters of the polymer dynamics. To this end we have calculated relevant correlation functions for the tube/reptation model and evaluated eq 9 accordingly. Many details of the theory underpinning the present analysis are given in the paper by Ball, Callaghan, and Samulski,[6] and the reader is referred to the derivations contained in that work. For the purpose of the present article we reproduce the key ideas in the next section.

The Doi–Edwards/de Gennes model and the correlation functions for dipolar fluctuations. In this paper we shall seek to apply the predictions of the reptation model for entangled polymer dynamics in analyzing experimental β-echo curves obtained as part of this work. This model, which is one of a number of competing descriptions of polymer motion, has the advantage of great simplicity and provides specific closed form expressions for the various modes of polymer translational motion. The lateral movements of an entangled polymer is thought to be restricted by the surrounding chains as though it were constrained by topology to diffuse in a "tube." The very existence of the tube in turn provides the link between the chain's translational diffusion—the nominally 1-dimensional Brownian motion of the polymer as it moves back and forth in the tube which thereby delineates its "primitive path" comprised of inter-entanglement path steps *a* (see Figure 1)—and its large-scale rotational modes and thus enables an estimation of the relevant reorientational correlation functions for dipolar fluctuations. It is not the purpose of the present pare to argue the virtue of the reptation picture *vis-à-vis* other descriptions of polymer dynamics. However, the model provides a natural starting point for our investigation of the utility of β and, in particular, the degree to which this function can provide insight regarding polymer motion.

The tube/reptation model has been described in detail elsewhere and we recap only the salient points. (Recently Doi[17] has succinctly described the essence of the model.) It is a mean field description in which Brownian motion is impeded by the topological constraints of surrounding chains.[3,8] For motion on a length scale intermediate between limits of the inter-entanglement distance, *a*, and polymer rms end-to-end length, *R*, the so-called reptation dynamics is characterized by 1-dimensional curvilinear diffusion in the tube. Beyond the distance *a*, the primitive path step size, the directed motion is initially Rouse-like[18] while at a greater length scale, and for times longer than the Rouse time τ_R, the motion corresponds to center-of-mass diffusion, directed along the tube primitive path, and characterized by the one-dimensional curvilinear diffusion coefficient $D_1 = k_BT/N\zeta$ where ζ is the segment friction and N is the number of Kuhn segments, of length *b*, per chain. For a Gaussian chain $R^2 = Nb^2 = Za^2$ where Z *is* the number of primitive path steps of size *a*. The number of Kuhn segments per primitive path is denoted $N_e = N/Z$ and corresponds to a chain length approximately half that of the critical molar mass for entanglement, M_c.

Once the polymer diffuses a distance on the order of its own length, tube disengagement effects allow 3-dimensional freedom in the center-of-mass diffusion while at distances smaller than the tube step size *a*, the motion corresponds to the internal modes of a free Rouse chain. These two respective long range and short-range processes are central to any understanding of the influence of dipolar interactions in polymer melts. The short-range motion is rapid but anisotropic in that it does not permit the spin pairs to sample all possible orientations. It thus has the effect of "pre-averaging" the dipolar interaction along *a*, leaving it considerably weaker in magnitude, but still available to be modulated by further motion and hence useful as a means of tracking slower modes of reorientation and, in particular, the reorientation associated with the slow curvilinear migrations along the tube. At the other extreme the tube disengagement, while much slower in comparison, represents the last act in the establishment of complete orientational freedom, the step by which orientational order is finally lost. Beyond that process, no dipolar interactions remain with which to track the polymeric diffusion.

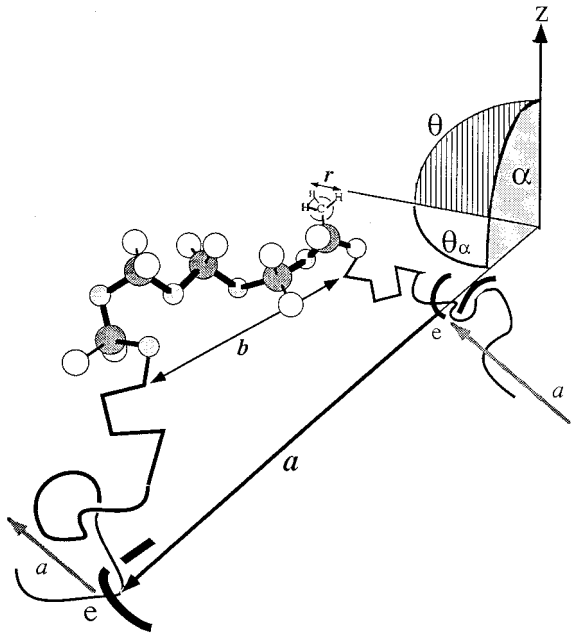

Figure 1. Schematic representation of a fragment of PDMS chain shown on several length scales simultaneously. On the atomistic scale the (freely jointed) Kuhn segment ***b*** is comprised of approximately five PDMS monomers. On a longer length scale, the contour of the Gaussian chain fragment is confined between consecutive entanglements, e, which in turn define the primitive path step ***a***, a director at orientation α relative to the *z*-axis. The proton dipolar interaction is determined by the instantaneous orientation of the vector ***r*** connecting a pair of protons within a methyl group. This orientation θ, the polar angle between ***r*** and the magnetic field direction (*z*-axis), can in turn be defined in terms of the angles α and θ_α, where the latter is the instantaneous orientation of ***r*** relative to its associated primitive path director. The dipolar interactions originating from the pairs of spins within a methyl group are "pre-averaged" along ***a*** by fast local motions—methyl group rotation, intra-Kuhn segment isomerization, and reorientations of ***b*** by (restricted) Rouse modes—to yield a residual proton second moment, $M_2 = M_2 (\langle P_2(\cos\theta_\alpha(t))\rangle_{fast})^2 \approx 10^5\ s^{-2}$.

The three characteristic times which subdivide the motional regimes are τ_e, the time taken for a segment to diffuse a distance *a*, the Rouse time, τ_R, and the tube disengagement time, τ_d. Note that $\tau_R = R^2/3\pi^2D_1$, $\tau_e = \tau_R/Z^2$, and $\tau_d = 3Z\tau_R$. The disengagement of tube segments is multiexponential process which can be represented by the fraction of tube remaining after time

t, namely

$$\Psi_{\text{tube}}(t) = \sum_{p\ \text{odd}} \frac{8}{\pi^2 p^2} \exp(-p^2 t/\tau_d) \qquad (11)$$

In accordance with the hierarchy of motion described above, the tube model predicts subdivision of motional regimes in terms of scaling laws involving the mean squared laboratory frame displacement of the polymer segments, $\Phi(t) = \langle(\mathbf{R}_n(t) - \mathbf{R}_n(0))^2\rangle$, where $\mathbf{R}_n$ is the coordinate of segment n and the ensemble average $\langle ... \rangle$ includes an average over segment number. These regimes are as follows:

I free Rouse motion:

$$t \lesssim \tau_e \quad \Phi(t) \lesssim a^2 \quad \Phi(t) \sim t^{1/2} \qquad (12.\text{I})$$

II Rouse motion constrained to the tube:

$$\tau_e \lesssim t \lesssim \tau_R \quad a^2 \lesssim \Phi(t) \lesssim Ra \quad \Phi(t) \sim t^{1/4} \qquad (12.\text{II})$$

III curvilinear diffusion in the tube:

$$\tau_R \lesssim t \lesssim \tau_d \quad Ra \lesssim \Phi(t) \lesssim R^2 \quad \Phi(t) \sim t^{1/2} \qquad (12.\text{III})$$

IV long-range center-of-mass motion:

$$\tau_d \lesssim t \quad R^2 \lesssim \Phi(t) \quad \Phi(t) \sim t^{1} \qquad (12.\text{IV})$$

We now summarize the effect of the corresponding rotational dynamics in each regime on the dipolar interaction. The first step in the dynamical hierarchy is that of regime I, wherein rapid local motions of the Gaussian chain section of end-to-end length a result in a reduced but finite dipolar interaction term. This "residual interaction" term shall be used to track the motion further up the hierarchy; its magnitude will be of great importance in determining the nature of motional averaging at higher levels. We therefore focus on this first step in some detail.

Figure 1 provides a schematic illustration of our model for dipolar interactions between proximate spin pairs. For a geminal proton spin pair in a methylene or the spin pairs within a methyl group, the interproton distance is the same, $r = 0.178$ nm. For such spins residing in a polymer chain, the characteristic dipolar interaction strength, $M_2^{1/2}$, is around 10^5 Hz. (The 90° orientation of r relative to the methyl C_3-axis results in an exact compensation of the additional contribution to $M_2^{1/2}$ from the second spin in a methyl group exercising rapid rotation.) Hence for those dipolar interactions stemming from either methylenes or (rotating) methyl groups, local motional averaging is only effective if it occurs on a time scale of around 10^{-6} s. This is very feasible however, as this time scale is quite slow compared with the time scale for local segmental motion ($\sim 10^{-10}$ s). From eq 2 it is clear that the dipolar frequency $\omega(t)$ will be substantially pre-averaged by the much faster local motions in $\theta(t)$ associated with the local modes, i.e., all motion from the scale of the internal processes within a Kuhn segment up to the "equilibration" Rouse modes characterized by time τ_e.

This pre-averaging may be expressed in terms of the reduced second moment

$$\bar{M}_2 = M_2 (\langle P_2(\cos \theta_\alpha(t))\rangle_{\text{fast}})^2 \qquad (13)$$

If we adopt the perspective of J−P Cohen-Addad,[19] for a Gaussian chain of N_e statistical units fixed at both ends, the internal motional averaging leads to $\langle P_2(\cos \theta_\alpha(t))\rangle_{\text{fast}} \approx N_e^{-1}$. Furthermore we take the view that the effect of the topological constraints surrounding the local tube segment is to impose a directional constraint akin to the fixing of end points of a section of chain of N_e units over a length a, a view which is clarified by thinking of the "end fixtures" as arising from physical entanglements separated by distance a (Figure 1).

We now turn our attention up the hierarchy to regimes II and III. The fast motional averaging due to regime I displacements leaves a substantially weakened residual dipolar interaction acting as though its director (i.e., the apparent internuclear vector for all spins in that step of the tube) were aligned with the local primitive path step a. We have shown in BCS that the higher level motion results in dipolar frequency time-correlation functions:

$$C(t) = \bar{M}_2 (t/\tau_e)^{-1/4} \quad \tau_e < t < \tau_R \qquad (14.\text{II})$$

$$C(t) = \bar{M}_2 (t/\tau_e)^{-1/4} (t/\tau_R)^{-1/4} \sum_{p\ \text{odd}} \frac{8}{\pi^2 p^2} \exp(-p^2 t/\tau_d) \quad \tau_R < t \qquad (14.\text{III})$$

Note that eq 14.III encompasses both regimes III and IV. From eq 14 the integrals needed to evaluate $\beta(2\tau,\tau)$ (see eqs 7 and 10) may be derived. While this is straightforward in the case when τ is entirely within regime II, for τ greater than $^1/_2\tau_R$, it is necessary to allow for appropriate crossovers in the expressions for $C(t')$ when carrying out any integration within the range from 0 to 2τ. In earlier work,[7] we approximated these integrals by assuming a regime III/IV correlation function across the entire time range. We now present exact expressions in which the correlation function is subdivided.

First Term:

$$\langle \phi(0,\tau)^2 \rangle = 2\int_0^\tau dt' \, (\tau - t') C(t')$$

For $\tau_e < t < \tau_R$ (regime II):

$$2\int_0^\tau dt' \, (\tau - t') C(t') = 1.524 \bar{M}_2 \tau_e^{1/4} \tau^{7/4} \qquad (15a)$$

For $\tau_R < t$ (regimes III and IV):

$$2\int_0^\tau dt' \, (\tau - t') C(t') = \frac{8}{3}\bar{M}_2 (\tau_e^{1/4} \tau_R^{3/4}) \tau - \frac{8}{7}\bar{M}_2 (\tau_e^{1/4} \tau_R^{7/4}) + 2\bar{M}_2 \sum_{p\ \text{odd}} \frac{8}{\pi^2 p^2} (\tau_e^{1/4} \tau_R^{1/4}) \alpha_p^{-3/2} [(2\alpha_p \tau - 1) \int_0^{(\alpha_p \tau)^{1/2}} dy \exp(y^2) + (\alpha_p \tau)^{1/2} \exp(-\alpha_p \tau) - (2\alpha_p \tau - 1) \int_0^{(\alpha_p \tau_R)^{1/2}} dy \exp(y^2) - (\alpha_p \tau_R)^{1/2} \exp(-\alpha_p \tau)] \qquad (15b)$$

Second Term:

$$\langle \phi(0,\tau)\phi(\tau,2\tau) \rangle = \int_0^\tau dt' \, t' C(t') + \int_\tau^{2\tau} dt' \, (2\tau - t') C(t')$$

For $\tau_e < t < {}^1/_2\tau_R$ (regime II):

$$\int_0^{\tau} dt'\, t'C(t') + \int_{\tau}^{2\tau} dt'\, (2\tau - t')C(t') = 1.039\, \bar{M}_2 \tau_e^{1/4} \tau^{7/4} \quad (16a)$$

For $^1/_2\tau_R < t < \tau_R$ (regime II/III transition):

$$\int_0^{\tau} dt'\, t'C(t') + \int_{\tau}^{2\tau} dt'\, (2\tau - t')C(t') = 1.143\bar{M}_2 \tau_e^{1/4} \tau^{7/4} - 1.922\bar{M}_2 \tau_e^{1/4} (\tau_R/2)^{7/4} + \frac{8}{3}\bar{M}_2 \tau_e^{1/4} \tau [\tau_R^{3/4} - \tau^{3/4}] + \bar{M}_2 \sum_{p\ \mathrm{odd}} \frac{8}{\pi^2 p^2} (\tau_e^{1/4} \tau_R^{1/4}) \alpha_p^{-3/2} [(2\alpha_p\tau)^{1/2} \exp(-2\alpha_p\tau) - \int_0^{(2\alpha_p\tau)^{1/2}} dy \exp(-y^2) - (\alpha_p\tau_R)^{1/2} \exp(-\alpha_p\tau_R) + \int_0^{(\alpha_p\tau_R)^{1/2}} dy \exp(-y^2) + 4\alpha_p\tau \int_{(\alpha_p\tau_R)^{1/2}}^{(2\alpha_p\tau)^{1/2}} dy \exp(-y^2)] \quad (16b)$$

For $\tau_R < t$ (regime III/IV):

$$\int_0^{\tau} dt'\, t'C(t') + \int_{\tau}^{2\tau} dt'\, (2\tau - t')C(t') = 1.143\bar{M}_2 \tau_e^{1/4} \tau_R^{7/4} - 1.922\bar{M}_2 \tau_e^{1/4} (\tau_R/2)^{7/4} + \bar{M}_2 \sum_{p\ \mathrm{odd}} \frac{8}{\pi^2 p^2} (\tau_e^{1/4} \tau_R^{1/4}) \alpha_p^{-3/2} [-2(\alpha_p\tau)^{1/2} \exp(-\alpha_p\tau) + 2\int_0^{(\alpha_p\tau)^{1/2}} dy \exp(-y^2) + (\alpha_p\tau_R)^{1/2} \exp(-\alpha_p\tau_R) + \int_0^{(\alpha_p\tau_R)^{1/2}} dy \exp(-y^2) + (2\alpha_p\tau)^{1/2} \exp(-2\alpha_p\tau) - \int_0^{(2\alpha_p\tau)^{1/2}} dy \exp(-y^2) + 4\alpha_p\tau \int_{(\alpha_p\tau)^{1/2}}^{(2\alpha_p\tau)^{1/2}} dy \exp(-y^2)] \quad (16c)$$

where $\alpha_p = p^2/\tau_d$.

The Shape of the β Function. The β function exhibits a number of interesting properties when used to study dipolar interactions: for example, its null value when the dipolar interactions are absent and the direct correspondence of its initial rate of rise with the average dipolar second moment. However, we believe that this function also exhibits a high degree of sensitivity to the precise nature of the dynamics, as expressed via the correlation function $C(t)$ and the consequent integrals which determine the phase factors of eqs 15 and 16. In particular, we would argue that this sensitivity is significantly greater than is found in the measured quantities for other NMR methods which provide information about the strength and fluctuations of dipolar interactions. To illustrate that point, we will consider just the maximum amplitude of $\beta(2\tau,\tau)$, a property which is independent of the interaction strength and which depends only on the functional form of the time dependence. Parts a−c of Figure 2 show three different plots of $\beta(2\tau,\tau)$ with three different correlation functions, namely, a simple exponential, a $t^{-1/4}$ power law, and a $t^{-1/2}$ power law. The respective maxima of $\beta(2\tau,\tau)$ for these correlation functions are 0.5, 0.28, and 0.16. In each case where the coefficient $\bar{M}_2$, which determines the strength of the correlation function, is changed, the initial rate of rise changes but the maximum of $\beta(2\tau,\tau)$ is unaffected.

Next, in Figure 2d we illustrate the power law behavior which characterizes the reptation correlation function in the absence of tube disengagement. In such a case $C(t)$ starts as $(\bar{M}_2)(t/\tau_e)^{-1/4}$ and then crosses over, at τ_R, to $(\bar{M}_2)(t/\tau_e)^{-1/4}(t/\tau_R)^{-1/4}$. In this example we illustrate the behavior of $\beta(2\tau,\tau)$ using a family of curves generated with different values of molar mass M and hence Rouse times $\tau_R = \kappa M^3/(3Z)$, where κ is some prefactor which reflects the dynamical rate constant. As expected the $\beta(2\tau,\tau)$ maximum begins at 0.28 for the largest molar masses where no Rouse transition is encountered in the observational time scale, and for which the power law exponent is $-^1/_4$. This maximum value then exhibits a crossover to 0.16 which is associated with the $t^{-1/4}$ to $t^{-1/2}$ transition at τ_R. Another feature of the $\tau < \tau_R$ regime is the invariance of the initial rate of rise of $\beta(2\tau,\tau)$ as M is varied, reflecting the fact that $\tau_e \sim M^0$. However, once crossover occurs the $(\tau_e\tau_R)^{1/4}$ coefficient introduces a molar mass dependence via $\tau_R \sim M^2$, and this is reflected in the varying initial slopes as M is decreased (decreasing line thickness in Figure 2d). This dependence of initial slope on τ_R occurs irrespective of the fact that the Rouse time is below the observational time scale τ. The physical basis of the observation that the short time scale Rouse modes influence the rise of $\beta(2\tau,\tau)$ on a longer time scale ($\tau \gg \tau_R$) derives from the fact that reptative displacements prior and after the Rouse time have differing motional averaging efficiencies. As a consequence the effective interaction strength, $(\bar{M}_2)$, depends on the extent of the evolution time prior to τ_R.

Hence we would argue that the observed maximum amplitude of the experimental $\beta(2\tau,\tau)$ data will give a clue as to the nature of the dynamics. But it is also important to note that this height will be sensitive to all dynamical regimes, not just that prevailing at the observational time scale τ. The reason for this is that $\beta(2\tau,\tau)$ involves a series of integrals of $C(t)$ over all past history from $t = 0$. A nice illustration of this point may be found in Figure 2d where the height of $\beta(2\tau,\tau)$ exceeds the asymptotic value of 0.16 at values of τ which exceed τ_R. The $t^{-1/2}$ power law plateau is only reached once $\tau \gg \tau_R$.

It is important to note that, whatever the value of τ_R, $\beta(2\tau,\tau)$ will always rise to a maximum value of 0.16 providing that the $t^{-1/2}$ power law behavior of regime III persists. Further reduction in this peak amplitude of $\beta(2\tau,\tau)$ will require the additional loss of correlation which occurs under tube disengagement.

Finally, we note that a direct application of the tube model in which it is assumed that $\tau_d = \kappa M^3$ implies that in principle, only two parameters, $\bar{M}_2$, the pre-averaged interaction strength, and κ the prefactor, are needed to specify $\beta(2\tau,\tau)$ in terms of the integrals in eqs 15 and 16 since existing knowledge of N_e (or M_e) and N (or M) will then enable us to calculate τ_R and τ_e from their interrelationships: $\tau_d = 3Z\tau_R$ and $\tau_e = \tau_R/Z^2$ with $Z = N/N_e$.

Experimental Section

Narrow MW distribution fractions of poly(dimethyl siloxane) (PDMS) were obtained from American Polymer Standards Corporation, Cincinnati, OH, and fractions of poly(ethylene oxide) were obtained from Polymer Laboratories, Church Stretton, U.K. (see Table 1 for data pertaining to these samples). For PDMS we also tabulate the respective number of entanglements, Z, determined from the entanglement molar mass, $M_e = M_c/2 = 10^4$; the tabulated Rouse times, τ_R, and disengagement times, τ_d are computed from a literature value of the equilibration time, $\tau_e = 7 \times 10^{-8}$s at 300 K.[20] The "entanglement" or "equilibration" time, τ_e, is related to the "segmental reorientation" time, τ_s, through $\tau_e = N_e^2\tau_s$. N_e is

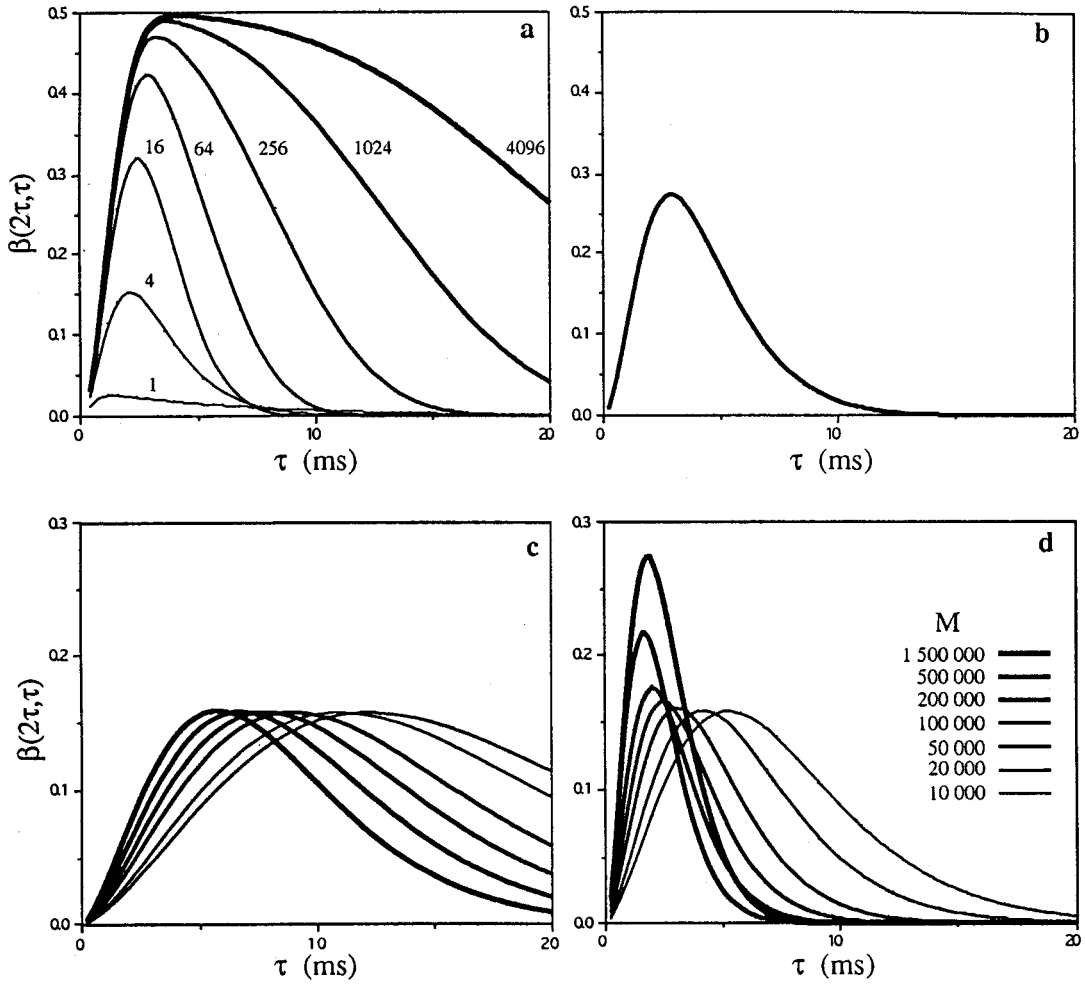

Figure 2. Plots of $\beta(2\tau,\tau)$ numerically evaluated from eq 9 are shown for several correlation functions: (a) $C(t) = \exp[-t/(4p\tau_c)]$, where $\bar{M}_2 = 2 \times 10^5$ s^{-2}, $\tau_c = 4 \times 10^{-4}$ s, and the integer factor p ranges from 1 to 4096 with increasing line thickness; (b) $C(t) = \bar{M}_2 t^{-1/4}$ where is an arbitrary prefactor; (c) $C(t) = \bar{M}_2 t^{-1/2}$ where the arbitrary prefactor decreases from left to right (with decreasing line thickness); (d) $C(t)$ starts as $\bar{M}_2(t/t_e)^{-1/4}$ (thick line) and then crosses over, at τ_R, to $\bar{M}_2(t/t_e)^{-1/4}(t/\tau_R)^{-1/4}$. The family of curves is generated with no disengagement ($\tau_{dis} = \infty$) for decreasing molar mass M and hence Rouse times, $\tau_R = \kappa M^3/(3Z)$, where the prefactor $\kappa = 1 \times 10^{-18}$ s, the equilibration time $\tau_e = \tau_R Z^{-2}$, and the number of entanglements Z is given by $Z = M/M_e$ using $M_e = 10^4$; the coefficient $\bar{M}_2 = 2 \times 10^5$ s^{-2} is held constant.

Table 1. Characteristics of PDMS Samples and PEO Samples Given in Terms of the Peak Molar Mass, M_p, and the Polydispersity, M_w/M_n; $M_e = M_c/2 = 10^4$ for PDMS

PDMS (American Polymer Standards Corporation)

$M_p = (M_w M_n)^{1/2}$	M_w/M_n	$Z = M_p/M_e$	$\tau_R = Z^2\tau_e$ (ms)	$\tau_d = 3Z\tau_R$ (ms)
1 350 000	1.42	135	1.30	520
840 000	1.56	84	0.50	130
540 000	1.42	54	0.20	33
357 000[a]	1.50	36	0.091	10
195 000	1.24	20	0.028	1.7
140 000	1.20	14	0.014	0.59
105 000	1.19	11	0.0086	0.29

PEO (Polymer Laboratories)

$M_p = (M_w Mn)^{1/2}$	M_w/M_n	$Z = M_p/M_e$[b]
847 000	1.16	292
400 000	1.08	138
246 000	1.09	85
105 000	1.06	36
56 300	1.05	19
23 000	1.08	8

[a] Polymer Laboratories. [b] $M_e = M_c/2 = 2.9 \times 10^3$.

the number of statistical segments spanning entanglements which in turn, can be found with $N_e = M_e/jm$, where j is the number of monomers per (Kuhn) statistical segment, and m (=75 Da) is the monomer molar mass. An estimate[21] of $j \approx 5$, gives $N_e \approx 27$. From this estimate one infers $\tau_s = 9.6 \times 10^{-11}$ s in agreement with value of $\tau_s = 9.8 \times 10^{-11}$ s derived from a fit of T_1 relaxation data (ref 20, Figure 1).

All NMR samples were prepared by placing into open-ended 2.5 mm diameter glass tubes, a column of polymer melt with a length of 2−3 mm. The glass tube was then placed into a 3 mm ID solenoidal rf coil so that the melt sample was centrally positioned in the most homogeneous region of the rf field. Temperature control was achieved using an air stream which passed through a jacket surrounding the coil. A thermocouple placed in this stream close to the coil was used to regulate the temperature via standard feedback.

^{1}H NMR experiments were carried out at 300 MHz using a Bruker AMX300 spectrometer and 89 mm vertical bore superconducting magnet. The pulse sequence used to generate the β-echo signal is shown in Figure 3. The echo is generated by a composite comprises of 90°and 45° rf pulses using a specialized phase cycling pattern, details of which can be found in ref 6. This cycle is completed in 24 separate steps and this was the standard number of acquisitions used per delay time, τ. It should be noted that the β-echo requires good rf homogeneity and accurate rf pulse durations in order to work well, and we have taken particular care before every measurement to optimize all pulse settings.

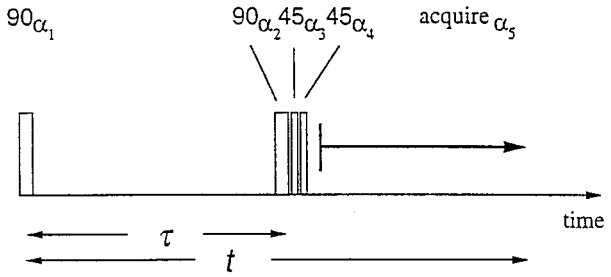

Figure 3. Radio frequency pulse sequence used to acquire the $\beta(t,\tau)$-echo function (see ref 6 for details about implementation). A series of 24 experiments are run where the τ value is changed from 0.05 to 20.0 ms and the 2τ value, $\beta(2\tau,\tau)$, is obtained for subsequent analysis.

Results and Discussion

Molar Mass Dependence for PDMS. In Figure 4a we show the experimental β-echo signals obtained for the PDMS samples at 300 K. Several key features are immediately apparent. First, the data exhibit declining maxima with decreasing M, which implies that disengagement is underway. Second, the β curve for the highest molar mass (GPC peak molar mass $M_p = 1.35 \times 10^6$ Da) rises to a maximum of 0.16, strongly suggsting that this system is exhibiting an asymptotic power law behavior characteristic of the regime III. That this particular polymer is experiencing only very slow disengagement is also suggested in the rather weak onset of disengagement in the $M_p = 0.84 \times 10^6$ Da data which then accelerates as M_p is further reduced. We have first attempted to fit the data by using eqs 15 and 16 and by adjusting $\bar{M}_2$ and the dynamical prefactor, κ. In the calculation of τ_d we have allowed for polydispersity by assigning to M the value of the peak molar mass, $M_p = (M_w M_n)^{1/2}$. The results at best fit are shown in Figure 4b where it is clear that despite the overall shape of the data being well-represented, the maximum theoretical value computed for β at the highest molar mass ($\beta \approx 0.19$ at $\tau \approx 3$ms) is well in excess of the regime III plateau of 0.16. As demonstrated in the theory section (see Figure 2d), such an enhanced amplitude indicates that the τ_R value for this polymer is too close to the prevailing experimental time scale (Table 1 suggests $\tau_R = 1.3$ ms). At this point we note that adjustment of the $\tau_d \sim M^3$ scaling exponent cannot rectify this problem. Furthermore we have found that accounting for polydispersity by using a superposition of β curves corresponding to the known molar mass distribution makes practically no difference to the fitted curves. Indeed we are only able to reproduce the observed data if we further modify the simple reptation model adaptation used here by shifting the position of the $t^{1/4}$ to $t^{1/2}$ transition further back in time than would be suggested by the Rouse value of $\tau_R = \tau_d/3Z$.

Figure 4c shows the result of a fit achieved by setting the $t^{1/4}$ to $t^{1/2}$ transition at a time shorter by a factor of 1/20 for all polymers ($\tau_R^{\text{effective}} = \tau_R/20$). The precise value of this factor is unimportant provided the extent of the shift is substantial. This represents a change in the corresponding length scale for the transition by a factor of $\sim 2 \approx 20^{1/4}$. We justify such an arbitrary change on the basis that this shift is common to all molar masses and can be considered to represent a small uncertainty in the precise length at which the center of mass Rouse motion predominates in the directed motion of the polymer within the curvilinear tube path. The significance of this shift is that it allows for an analysis

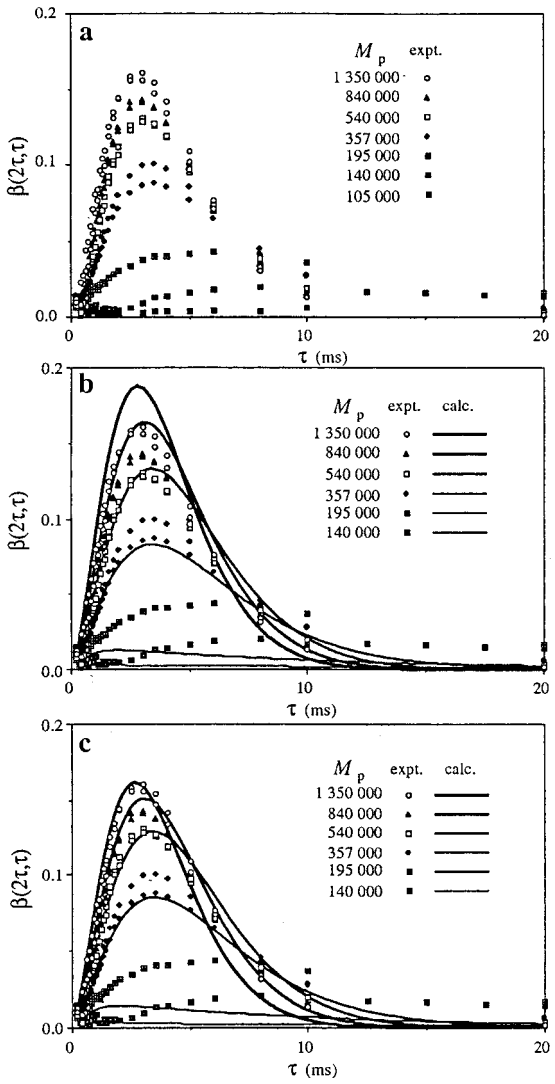

Figure 4. Experimental values of $\beta(2\tau,\tau)$ for PDMS contrasted with calculated values using the full reptation correlation function: (a) data at 300 K as a function of molar mass M_p, where replicated experiments show the uncertainty in the measurements for a given molar mass; (b) calculated $\beta(2\tau,\tau)$ (solid curves) for the full reptation correlation function (eqs 14−16), where the calculation uses $\bar{M}_2 = 1.7 \times 10^6$ s^{-2} and the ideal Rouse times, $\tau_R = \kappa M^3/(3Z)$, with the prefactor $\kappa = (0.9 \pm 0.2) \times 10^{-19}$ s and Z is given by $Z = M_p/M_e$ using $M_e = 10^4$; (c) calculated $\beta(2\tau,\tau)$ (solid curves) for the full reptation correlation function using an effective Rouse time, $\tau_R/20$, $\bar{M}_2 = (3.3 \pm 0.2) \times 10^6$ s^{-2} and $\kappa = (1.0 \pm 0.2) \times 10^{19}$ s.

of the data in which several major elements of the reptation model play a key role. We reiterate that the effects of tube disengagement with decreasing PDMS molar mass are apparent as stated previously but, in addition, the existence of a prior Rouse transition is required by the declining initial slopes of β as M decreases (recall discussion of Figure 2d).

The curves shown in Figure 4(c) were optimized for best fit by adjusting the parameters $\bar{M}_2$ and κ. The best fit yields $\bar{M}_2 = 3.3 \times 10^6$ s^{-2} and $\kappa = 1.0 \times 10^{-19}$ s, respectively. While the fits shown in Figure 4c well represent the data for the highest M_p values of 1 350 000, 840 000, 540 000, and 357 000 Da, the representation is much poorer at lower molar masses. One possible source of this discrepancy might be an incorrect assumption of the value of 3 in the τ_d molar mass scaling: $\tau_d \sim M^3$. While our data are indeed sensitive to this

exponent, no adjustment of this value alone can provide a good quality of fit across the entire range of molar mass (see below). Indeed, it would appear that below 357 000, factors other than the reptation correlation function of eq 16 are influential in determining the strength of the residual dipolar interaction. In simple terms it would appear that as the strength of the dipolar interaction weakens with reducing chain length (and hence increasingly rapid motional averaging), the spins start to exhibit sensitivity to a new, and much weaker, dipolar interaction term whose scaling with mass is slower than M^3. One obvious candidate for such a weak residual term is the effect of long-range dipolar interactions between protons situated in different polymer chains—*inter*molecular contributions.

Intermolecular dipolar interactions are known to contribute to the proton spin−lattice relaxation in simple liquids;[12] it is also substantial in polymer melts, glasses, and crystals where considerable interspersion among chains is inferred.[22] Our model for how such (preaveraged) intermolecular dipolar interactions contribute to β is as follows: If we were to assume a completely uniform spin density, then symmetry considerations would dictate that the integrated effect of all dipolar interactions from distance spins within in a sphere centered on the spin of interest would average to zero. Note, however, that the symmetry of the spin disposition is crucial. While the dipolar interaction arising from spins situated on any surrounding spherical shell of radius r is reduced by r^{-3}, the numbers of spins increases as r^2 dr, and so the integral is logarithmic. This effect is well-known in high-resolution NMR in liquids where the symmetry breaking effect of magnetic field gradients can reveal significant long-range dipolar interactions.[23] We argue that in a polymer melt the spin density is far from uniform because of the influence of microvoids, a consequence of free volume heterogeneity. Such voids have been implicated before to interpret NMR observations in polymer melts and have been suggested to lead to local susceptibility inhomogeneity effects which broaden the NMR line width.[10]

Our picture therefore is based on the idea that a much weaker intermolecular spin dipolar interaction is present and that this will fluctuate as the distant spin-bearing segment migrates. The key ideas behind the model are illustrated in Figure 5. For simplicity we shall assume that the correlation function for this process is exponential and set about estimating the correlation time. We shall first integrate interchain interactions. Given that the pre-averaging process means that we may neglect all intrachain dipolar interactions up to the length scale of the primitive path step, a, we shall also use this distance as the starting point for our consideration of (preaveraged) interchain dipolar interactions. Consequently we integrate starting at a distance on the order of a and up to the cutoff radius l_c, beyond which the density of the spins is taken to be uniform. This latter cutoff has the effect of removing the logarithmic divergence. The correlation time may be estimated for each distant spin pair by estimating the time taken to remain within a "coherence volume" such that the internuclear vector does not change its orientation significantly. This is tantamount to requiring that spins at starting separation r should have moved no further than r in a time t. By noting that such a laboratory frame displacement requires a tube curvilinear displacement s such that $as = r^2$, we find that the probability that pair of segments remains within the coherence volume is the just the error function

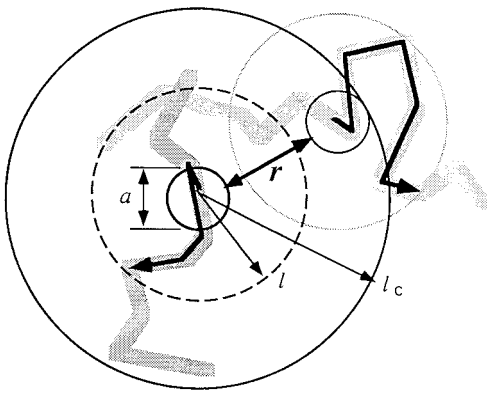

Figure 5. Pair of neighboring chain primitive paths and the diffusion trajectory of specific segments in each (bold arrows). Pre-averaged intermolecular dipolar interactions between spins on respective step segments are separated by a distance $\boldsymbol{r}$ and evolve as the distance/orientation changes as the chains diffuse. Such intermolecular interactions are considered over a spherical volume element of radius l and summed out to some cutoff distance l_c.

$$f(r) = \mathrm{erf}(x) = (4\pi D_c t)^{-1/2}\, 2 \int_0^{r^2/a} \exp(-s^2/4D_c t)\, \mathrm{d}s \tag{17}$$

where $x = r^2/(a(4D_c t)^{1/2})$. Next we assume that the intersegment M_2 will be determined by an integral involving only those spins which have not diffused out of the coherence volume, namely

$$[\int_a^{l_c} f(r)\, r^{-3} 2\pi r^2\, \mathrm{d}r]^2$$

We can gain a phenomenological estimate of this integral by assuming that the residual intersegment second moment will be dominated by a characteristic length somewhere between the limits a and l_c, a distance which we will call l. Hence the dominant correlation time will be that required for diffusion by a distance l where l is independent of molecular mass. If the cutoff distance is less than a coil radius, then the motion will be directed Rouse motion and the correlation time will be that required for curvilinear diffusion by a distance s such that $as = l^2$. Hence, τ_c is $(l^4/a^2 4D_c) \sim M^1$. If the cutoff distance is greater than the coil radius, then the slower reptative center of mass motion will play a role and $\tau_c \sim M^2$.

We therefore handle these weak intermolecular interactions by allowing for a residual interpair second moment, weaker than that due to the pre-averaged intrapair value, $\bar{M}_2$, by a factor γ, and with an exponential correlation function whose correlation time is given by $\tau_c = k_2 M^z$ where $1 < z < 2$. Then the total β-echo signal at $t = 2\tau$ is calculated using eq 9 and adding additional terms to the phase correlations $\langle \phi(0,\tau)^2 \rangle$ and $\langle \phi(0,\tau)\phi(\tau,2\tau) \rangle$, corresponding to the contribution from the intersegment interaction. These utilize the exponential correlation form[7]

$$\langle \phi(0,\tau)^2 \rangle = 2\gamma \bar{M}_2 \tau_c^{\,2} [\exp(-\tau/\tau_c) - 1 + \tau/\tau_c] \tag{18a}$$

$$\langle \phi(0,\tau)\phi(\tau,2\tau) \rangle = \gamma \bar{M}_2 \tau_c^{\,2} [1 - 2\exp(-\tau/\tau_c) + \exp(-2\tau/\tau_c)] \tag{18b}$$

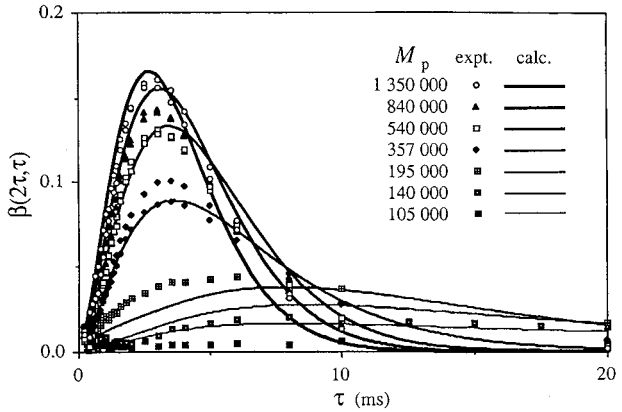

Figure 6. Calculated $\beta(2\tau,\tau)$ (solid curves) for the full reptation correlation function plus an intermolecular contributions (eq 18) with an effective Rouse time, $\tau_R/20$. $\bar{M}_2 = (3.6 \pm 0.2) \times 10^6$ s^{-2} (the effective residual second moment is $\bar{M}_2 = (1.7 \pm 0.1) \times 10^6$ s^{-2}) and the prefactor $\kappa = (1.0 \pm 0.2) \times 10^{-19}$ s. To evaluate intermolecular interactions, we employ $\gamma = 0.0009 \pm 0.0001$ with $\tau_c = k_2 M^{1.5}$ where $k_2 = 8 \times 10^{-11}$ s.

Figure 6 shows a fit to the PDMS data in which this new term is incorporated. The admixture coefficient, γ, required to provide a significant β-echo signal for the lower molar masses is very small, and in consequence, the perturbation to the preexisting good fits to high mass data due to the dominant intramolecular interaction is minimal. In particular the data is quite well represented by the values $\gamma \approx 0.001$ and $k_2 = 8 \times 10^{-11}$ s with $z = 1.5$.

Using these values along with the relationship $\tau_c \sim (l^4/a^2 4D_c)$, we may estimate the correlation length l. For example, for representative molar masses in the range 200 000−500 000, the length of l is on the order of $5a$. This dimension is close to a coil radius for polymers in this range, and so the fitted exponent of $z = 1.5$, falling between the scaling limits of 1 and 2 for directed Rouse and long-range center of mass diffusion, appears quite reasonable.

At this point we are able to return to the fits to establish whether a small change in the molar mass scaling exponent for τ_d can be detected in the fit quality. Before we examine this we note another refinement—the absence of residual dipolar interactions associated with the chain ends. Blocks of monomers beyond the last (and before the first) topological entanglement exercise essentially isotropic reorientational motion on the relevant experimental time scale and the motion of the chain's "end blocks" is unencumbered in the entangled melt.[24] Hence there are no (residual) dipolar interactions from a fraction of the chain, $p = 2M_e/M_p$. This influences the absolute intensity of the total β-echo signal by the factor $(1 - p)$, respectively, for β while, in addition, the strength of the intersegment dipolar interaction in eq 18 is reduced by the factor $(1 - p)$. The magnitude of these chain end corrections can be inferred by looking at the ideal reptation model result with $\tau_d \sim M^3$ (Figure 7a solid lines); the changes relative to calculations without such corrections (Figure 6) are small and most prominent at low molar mass (dotted lines in Figure 7a).

A more substantive influence on calculations in shown in Figure 7b, where we show the theoretical β-echo signals using $\tau_d \sim M^{3.4}$, the molar mass scaling thought to apply to reptating chains wherein chain end fluctuations are included.[17,25] The calculated curves shown in Figure 7 for fits using exponents of 3.0 and 3.4,

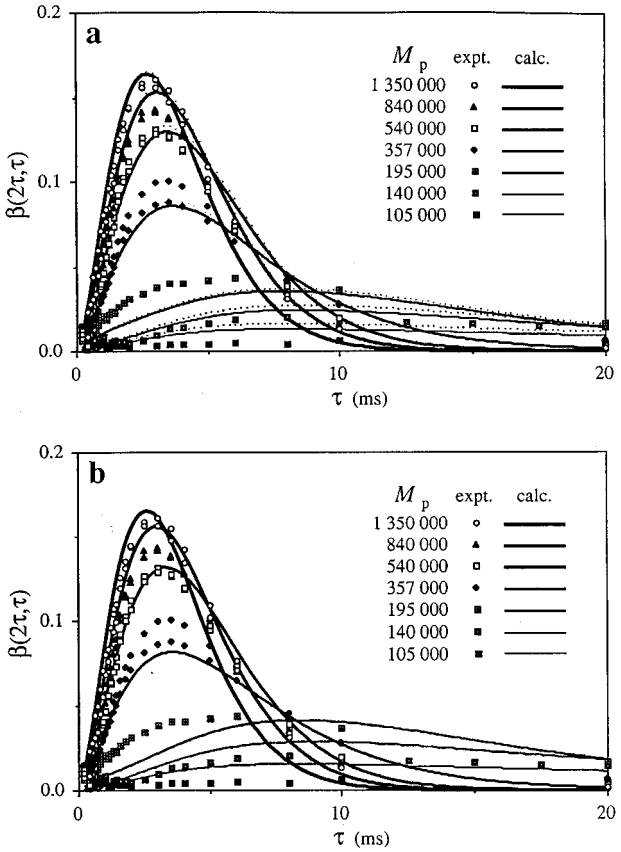

Figure 7. Calculated β (solid curves) for the full reptation correlation function plus intermolecular contributions (eq 18) with an effective Rouse time, $\tau_R/20$ and corrected for an absence of residual dipolar interactions associated with both ends of the chain. I.e., the residual interactions are completely averaged for the fraction $p = 2M_e/M_p$ of the chain (chain ends). Key: (a) $\tau_d \sim M^3$ and $\bar{M}_2 = (3.6 \pm 0.2) \times 10^6$ s^{-2} (effective residual second moment, $\bar{M}_2 = (1.7 \pm 0.1) \times 10^6$ s^{-2}) and the prefactor $\kappa = (8.0 \pm 0.2) \times 10^{-20}$ s; for the intermolecular interactions we employ $\gamma = 0.0011 \pm 0.0001$ with $\tau_c = k_2 M^{1.5}$ where $k_2 = 8 \times 10^{-11}$ s. (b) $\tau_d \sim M^{3.4}$ and $\bar{M}_2 = (3.8 \pm 0.2) \times 10^6$ s^{-2} (effective residual second moment, $\bar{M}_2 = (1.8 \pm 0.1) \times 10^6$ s^{-2}) and the prefactor $\kappa = (540000^{-0.4})(8.0 \pm 0.2) \times 10^{-20}$ s; $\gamma = 0.0012 \pm 0.0001$ with $\tau_c = k_2 M^{1.5}$ where $k_2 = 8 \times 10^{-11}$ s.

respectively, were obtained in each case by optimizing the agreement between theory and experiment; the values of the prefactor κ and the residual second moment admixture coefficient, γ, are adjusted for best fit. The $M^{3.4}$ molar mass scaling gives a noticeably poorer fit to the data, thus indicating the sensitivity of the β-echo signal to the choice of exponent and reinforcing the choice of the standard Doi−Edwards−de Gennes exponent of 3.0.

Finally in Figure 8 we let the molar mass scaling of τ_d vary to give the best fit to the data. In the two cases of intermolecular scaling that we examine, $\tau_c = k_2 M^z$ where $z = 1.5$ and $z = 2.0$ (parts a and b of Figure 8), we find that the best fit corresponds to $\tau_d \sim M^{2.6}$, a value smaller than the Doi−Edwards−de Gennes exponent of 3.0.

Temperature Dependence for PDMS. We have also investigated the temperature dependence of the β-echo signal for the 1.6×10^6 dalton sample of PDMS. The results over the range 240−390 K are shown in Figure 9a. A dramatic variation is apparent, and we are able to fit the data (solid lines) by varying the prefactor κ which governs the dynamics of all the

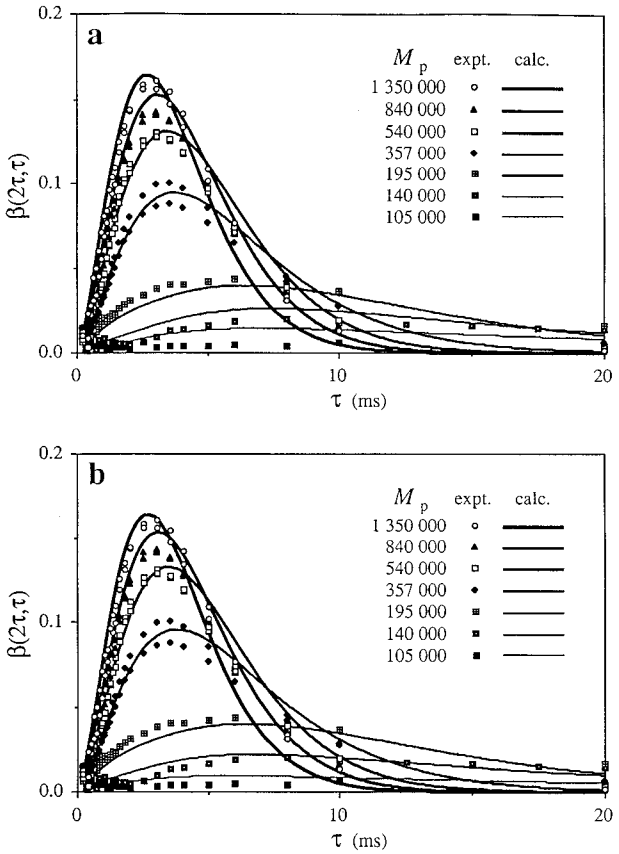

Figure 8. Calculated β (solid curves) for the full reptation correlation function where the molar mass scaling of the intramolecular (and intermolecular) interactions are optimized. The effective Rouse time is $\tau_R/20$, and chain end corrections are included. Key: (a) $\tau_d \sim M^{2.6}$, $\bar{M}_2 = (3.6 \pm 0.2) \times 10^6$ s^{-2} and the prefactor $\kappa = (540000^{-0.4})(8.0 \pm 0.2) \times 10^{-20}$ s; we use $\gamma = 0.0013 \pm 0.0001$ with $\tau_c = k_2 M^{1.5}$ where $k_2 = 8 \times 10^{-11}$ s. (b) $\tau_d \sim M^{2.6}$, $\bar{M}_2 = (3.6 \pm 0.2) \times 10^6$ s^{-2} and the prefactor $\kappa = (540000^{-0.4})(8.0 \pm 0.2) \times 10^{-20}$ s; we use $\gamma = 0.0013 \pm 0.0001$ with $\tau_c = k_2 M^{2.0}$ where $k_2 = 8 \times 10^{-13}$ s.

characteristic relaxation time scales; we use a fitting procedure similar to that used in Figure 6, i.e., the full reptation correlation function with $\tau_d \sim M^{3.0}$. These prefactors can in turn be analyzed so as to test for an Arrhenius dependence on temperature, as shown in Figure 9b. The Arrhenius fit is good and yields an activation energy of 13 kJ mol^{-1}. This activation energy agrees well with the value 16 ± 1 kJ mol^{-1} obtained more than 3 decades ago by Allen from viscosity measurements of PDMS melts.[26]

Molar Mass Dependence for PEO. We have carried out β-echo signal measurements on a range of monodisperse poly(ethylene oxide) samples (PEO) as listed in Table 1. These experiments were performed with a sample temperature of 90 °C, a value which is limited by apparent polymer degradation at temperatures in excess of 100 °C. The results are plotted in Figure 10. Once again the data show a characteristic variation in the shape of the β function as the molar mass is varied. However in this case, a fit using the Doi−Edwards−de Gennes correlation functions, as expressed in eqs 15 and 16, was not as successful as in the case of PDMS. In particular the variation with molar mass was less strong than predicted by the M^3 tube disengagement scaling exponent. This could be accounted for in part by a very large residual second moment admixture coefficient, γ, as shown in the fitted

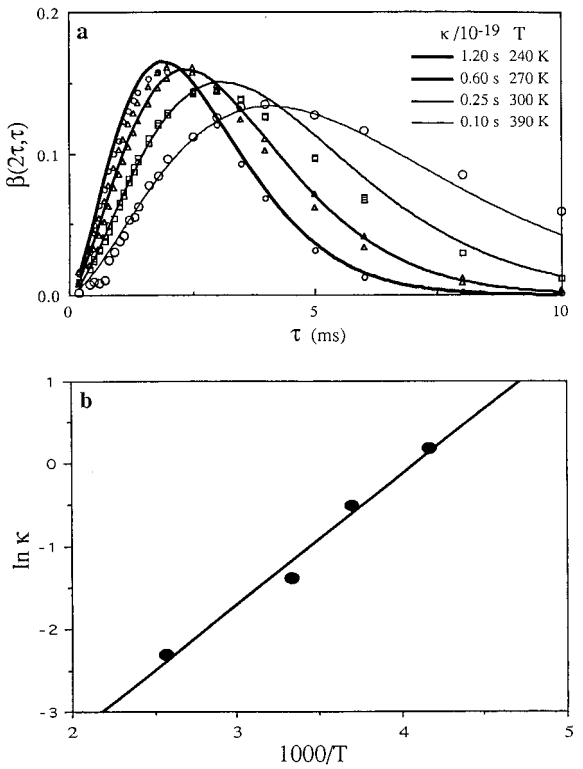

Figure 9. Temperature dependence of $\beta(2\tau,\tau)$ for PDMS (M_p = 1 350 000) for the range 240 to 390 K. (a) Experimental data (symbols) and fits (solid curves) for the reptation correlation function used to analyze the data in Figure 6 with the prefactor κ as the sole adjustable parameter; (b) Semilog plot of κ vs $10^3/T$, yielding a slope 1.577 ($R^2 = 0.983$) that corresponds to an activation energy of 13 kJ mol^{-1}.

curves superposed on the data in Figure 10a, although there exists no obvious physical justification for this contribution being so very much larger than in the case of PDMS.

Alternatively we can avoid any assumption regarding molar mass scaling in the terminal relaxation time, τ_d, and simply fit this value a priori, leaving the Rouse and equilibration times as given by the Doi−Edwards model (noting that the influence of these latter times is second order in the fits to the β function). The resultant fits to the data are quite good (Figure 10b), a fact which gives us some confidence in the physical description of the dipolar correlation function. However, as apparent in Figure 10c, the values of τ_d so obtained do not at all follow a M^3 scaling law below 400 000 Da, the observed disengagement times being greatly in excess of those predicted by reptation theory. We interpret this discrepancy as arising from the proximity of the melting transition of PEO at 67 °C; its glass transition is −67 °C. In contrast, PDMS exhibits no melting transition and has a glass transition temperature at −123 C. We infer that it is necessary to work at temperatures well in excess of melting (and glass transition) temperatures if the reptation model for polymer melts is to provide a good description of chain motion.

Conclusions

We would point out that in the present work the absence of scalar spin−spin interactions was a major simplifying factor. If the method is to be used with polymers whose spin systems exhibit J couplings, then the influence of these terms on the shape of the β function may need to be addressed. One way of sepa-

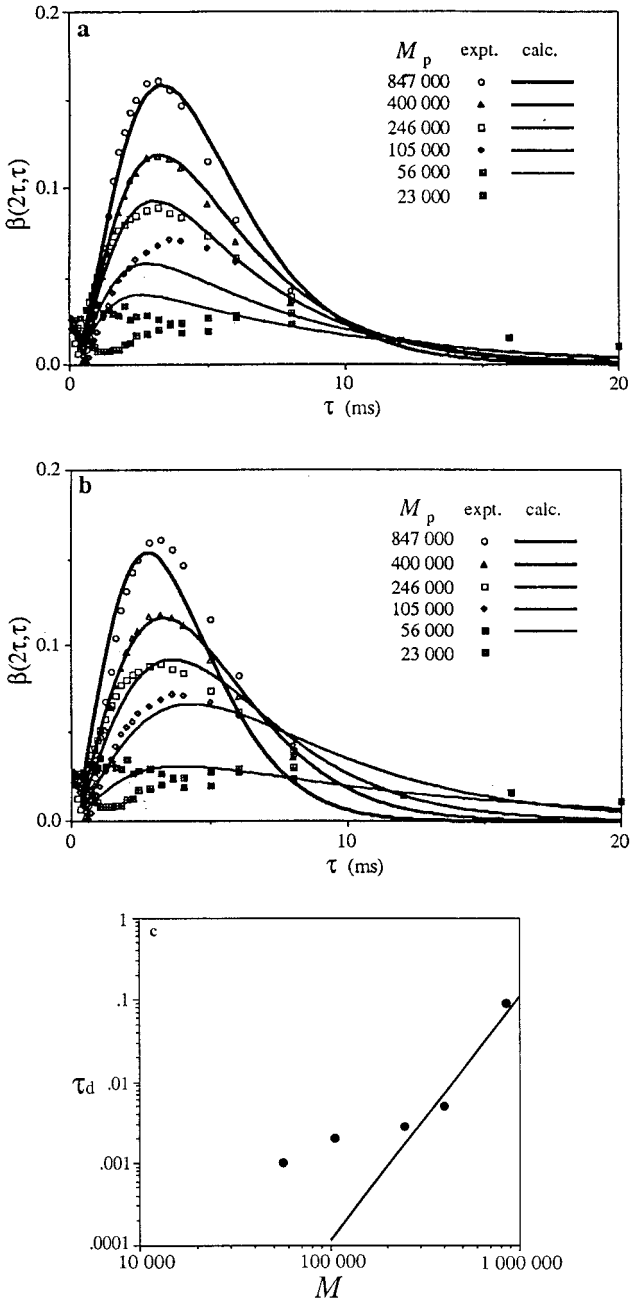

Figure 10. Molar mass dependence of $\beta(2\tau,\tau)$ for PEO at 90 °C. Key: (a) experimental β-echo signal (symbols) and fits (solid curves) for the reptation correlation function with $\tau_d \sim M^3$, as used to analyze the data in Figure 6, where $\bar{M}_2 = 2.0 \times 10^6$ s^{-2}, $\kappa = (1.0 \pm 0.2) \times 10^{-19}$ s, and $\gamma = 0.2$ with $\tau_c = k_2 M^{0.4}$, where $k_2 = 5.5 \times 10^{-6}$ s in the computation of intermolecular interactions; (b) experimental β-echo signal (symbols) and fits (solid curves) for the reptation correlation function with with τ_d used a fitted variable at each molar mass and $\tau_R = \kappa M^3/(3Z)$ and $\tau_e = \tau_R Z^{-2}$ with $\bar{M}_2 = 2.3 \times 10^7$ s^{-2}, and $\kappa = 1.0 \pm 0.2 \times 10^{-19}$ s (there is no contribution from intermolecular interactions, $\gamma = 0.0$); (c) log−log plot of the optimized τ_d values (obtained in part b) vs the molar mass M, where the straight line has a slope of 3.0.

rating the spin−spin and dipolar terms might be to utilize the strong temperature dependence of the latter. Furthermore, the fact that the magnitudes of the spin−spin couplings will, in each case, be well-known and that they exhibit molar mass independence should make any allowance for their effects relatively simple to incorporate into an analysis of the β-echo function.

The results obtained in this study on PDMS and PEO melts clearly illustrate that the β-echo function provides a sensitive test of polymer chain dynamics. The modulation of proton dipolar interactions which results as the polymer segments migrate can be directly related, via an orientational correlation function, to the appropriate model for chain dynamics. Note however, that the closed-form expression (eq 9) relating the experimental data to model correlation functions was derived by assuming that the modulation of the dipolar interactions is a Gaussian distributed process.[7] In this work we have chosen to work with the classical Doi−Edwards−de Gennes reptation model. While the results obtained for PDMS are broadly consistent with that model, we note that other theories which predict a hierarchy of chain motion and time scales could well be adapted to enable a satisfactory fit. In particular, the renormalized Rouse model of Schweizer[27] reproduces many of the segmental mean-squared displacement scaling regimes of the reptation model without the need for the a priori tube assumption. However the Doi−Edwards−de Gennes model has the distinct advantage that it generates closed form analytic expressions for the polymer dynamics right across the range of characteristic time scales while the crossover times themselves are well-defined in terms of the fundamental assumptions and parameters. Consequently, this model is the natural candidate for any initial test using a new experimental method which depends on a calculation deriving from the correlation functions for the motion.

The fitted parameters which result from this work agree reasonably well with those obtained by other methods. For example, the prefactor $\kappa = 1.0 \times 10^{-19}$ s^{-1} dalton^{-3} gives τ_d values within a factor of 2 of those calculated (see Table 1) using a literature value of the equilibration time.[20] The measured residual second moment of 3.3×10^6 s^{-2} may be rationalized as follows: A randomly oriented array of rapidly rotating methyl groups yields a static second moment $M_2 = 8.0 \times 10^9$ s^{-2} while the local averaging, $g(N_b)$, within the Kuhn statistical segment consisting of N_b monomers may be plausibly estimated[21] as $g(N_b = 5) \approx 0.4$. The pre-averaging for the Gaussian chain of N_e segments leads to a further reduction for the residual dipolar interaction of $(N_e)^{-1}$. As indicated above, we find $(N_e) \approx 27$ whence we expect $\bar{M}_2 = 27^{-2}\,(0.4)^2(8.0 \times 10^9)$ s^{-2} $= 1.8 \times 10^6$ s^{-2}, which is close to the measured value.

In the PDMS study the reptation model works reasonably well, provided that some allowance is made for an effective Rouse time and a weak intermolecular dipolar interaction. The former suggests that the connection between the return to origin probability affected by translational diffusion along the primitive path and rotational reorientation—substantive angular reorientations of the local path step director—may require additional analysis. While the latter intermolecular dipolar allowance is quite physical, its existence is unfortunate to the extent that the slower fluctuations associated with these more distant interactions tend to mask the effects of tube disengagement once the polymer dimension is sufficiently small, and in particular when the number of tube steps, Z, is less than $(l/a)^2$ where l is the effective range of the second-order interactions. In the present instance, that crossover appears to occur for $Z \sim 20$. Given that the tube model can only work for a sufficiently large number of entanglements, this constraint need not prove too limiting.

Moreover, the intermolecular dipolar interaction can be experimentally removed with isotopic dilution measurements using (identical molar mass) perdeuterated PDMS as the "solvent" for protonated chains.

Acknowledgment. We thank Robin Ball and Michael Rubinstein for discussions of our analysis. E.T.S. wishes to acknowledge support from the National Science Foundation (DMR-9412701) and the John Simon Guggenheim Foundation; P.T.C. acknowledges support from the New Zealand Foundation for Research, Science, and Technology.

References and Notes

(1) Powles, J. G.; Hartland, A.; Kail, J. A E. *J. Polym. Sci.* **1961**, *55*, 361−380.
(2) Powles, J. G.; Hartland, A. *Nature* **1960**, *186*, 26.
(3) de Gennes, P.-G. *J. Chem. Phys.* **1971**, *55*, 572.
(4) Cohen Addad, J.-P. *J. Chem. Phys.* **1974**, *60*, 2440.
(5) Cohen Addad, J.-P. *Prog. NMR Spectrosc.* **1993**, *25*, 1 and references therein.
(6) Callaghan, P. T.; Samulski, E. T. *Macromolecules* **1997**, *30*, 113.
(7) Ball, R. C.; Callaghan, P. T.; Samulski *J. Chem. Phys.* **1997**, *106*, 7352.
(8) Doi M.; Edwards, S. F. *The Theory of Polymer Dynamics*; Clarendon: Oxford, England 1986.
(9) It is customary to lump the anisotropic part of *J* into direct dipolar coupling constants in cases where it is measurable. See: Buckingham, A. D.; McLauchlan, K. A. *Prog. NMR Spectrosc.* **1967**, *2*, Chapter 2.
(10) Bachus, R.; Kimmich, R. *Polym. Commun.* **1983**, *24*, 317.
(11) Hahn, E. L. *Phys. Rev.* **1950**, *80*, 580.
(12) Abragam, A. *The Principles of Nuclear Magnetism*, Oxford University Press: Oxford, England, 1961.
(13) Kimmich, R.; Schnur, G.; Kopf, M. *Prog. NMR Spectrosc.* **1988**, *20*, 385. Kimmich, R.; Weber, H. W. *J. Chem. Phys.* **1993**, *98*, 5847.
(14) Anderson, P. W.; Weiss, P. R. *Rev. Mod. Phys.* **1953**, *25*, 269.
(15) Addad, J. P. C.; Pellicioli, L.; Nesselder, J. J. H. *Polym. Gels and Networks* **1997**, *5*, 201.
(16) Collignon, J.; Sillescu, H.; Spiess, H. W. *Colloid Polym. Sci.* **1981**, *259*, 220.
(17) Doi, M. *Introduction to Polymer Physics*; Oxford University Press: Oxford, England, 1996.
(18) Rouse, P. E. *J. Chem. Phys.* **1953**, *21*, 1272.
(19) Cohen Addad, J.-P. *J. Chem. Phys.* **1976**, *64*, 3438.
(20) Weber, H. W. Kimmich, R. *Macromolecules* **1993**, *26*, 2597.
(21) Poon, C.-D.; Samulski, E. T. *J. Non-Cryst. Solids* **1991**, *131*−*133*, 509.
(22) Wallenberg, B.; Sillescu, H. *Makromol. Chem.* **1977**, *178*, 2401. Cukier, R.; Natarajan, K.; Samulski, E. T. *Nature* **1978**, *275*, 527.
(23) Lee, S.; Richter, W.; Vathyam, S.; Warren, W. S. *J. Chem. Phys.* **1996**, *105*, 874.
(24) Kimmich, R.; Fischer, E.; Callaghan, P. T.; Fatkullin, N. *J. Magn. Reson.* **1995**, *A117*, 53.
(25) Rubinstein, M. *Theoretical Challenges in the Dynamics of Complex Fluids*; McLeish, T., Ed.; Kluwer Academic Publishers: Dorchecht, The Netherlands, 1997; p 21.
(26) Allen, G. *J. Appl. Chem.* **1964**, *14*, 1.
(27) Schweitzer, K. S. *J. Chem. Phys.* **1989**, *91*, 5822.

MA9715029